SECTION 4
COMBINED MLR MODEL FOR JAPANESE AND U.S. CASE HISTORIES

4.1 Earthquake Factors

The site-specific models developed for Niigata and Noshiro, Japan, were adjusted for a wider range of seismic and site conditions by including the U.S. data in the analyses. Youd and Perkins (1987), in developing the LSI model, proposed that displacement is a function of the amplitude, **A**, and duration, **D**, of strong ground motion.

$$D_H = f(A, D) \qquad (4.1.1)$$

where:
A = peak horizontal ground acceleration (in decimal fraction of g).
D = time interval between the first horizontal 0.05 g peak to the last 0.05 g peak recorded by a strong motion instrument (in seconds).

Unfortunately, strong motion records were not available for many of the lateral spread sites listed in Table 3-1. For these uninstrumented sites, **A** and **D** were estimated from empirical relationships based on earthquake magnitude, **M**, and the log of the distance to the seismic energy source, **LOG R** (Joyner and Boore, 1988; Youd and Perkins, 1987; Krinitzsky and Chang, 1988b; Appendix 1).

In addition to **A** and **D**, Youd and Perkins showed that D_H is a function of **M** and attenuates logarithmically with increasing **R**.

$$D_H = f(M, LOG\ R) \qquad (4.1.2)$$

where:
M = moment magnitude, M_w.
R = horizontal distance from the seismic source (in km).

The moment magnitude, M_w, is commonly used to represent **M** for these type of analyses because M_w is a better estimate of the amount of seismic energy released by a given earthquake than other measures of earthquake magnitude, especially for $M > 8.0$ events (Kanamori, 1978). Other earthquake magnitude measures such as the local magnitude, M_L, and the surface wave magnitude, M_s, are approximately equivalent to M_w for $6 \leq M \leq 8$ earthquakes (Krinitzsky and Chang, 1988b).

The distance from the seismic source, **R**, is measured as the horizontal distance from the site in question to the nearest point on a surface projection of the fault rupture zone. Epicentral distances may be adequate estimates of **R** for $M \leq 6$ earthquakes, but should not be used for larger earthquakes. Earthquakes with $M > 6$ are generally associated with large fault rupture zones that are not adequately characterized by a single point, such as the epicenter. Source zones for strike-slip and normal faults are usually delineated by a band that incorporates surface ruptures associated with recent (i.e., Holocene) faulting events. For these type of faults, which are common in the western U.S., source distances are measured horizontally from the nearest edge of the surface rupture zone to the site in question. For reverse faults, shallow-angle thrusts, and subduction-zone earthquakes, the associated zone of tectonic crustal uplift generally delineates the surface projection of the seismic source. For these type of faults, the source distance is measured from the nearest point of the tectonic uplift zone to the site in question.

Our preliminary regression analyses of the combined U.S. and Japanese data indicated that MLR models based on **M** and **LOG R** yield R^2 values that are about 10 to 15 percent higher than models based on **A** and **D**. Thus, we chose to use **M** and **LOG R** in subsequent models. However, we do not wish to imply that **M** and **LOG R** are better measures of seismic energy than instrumentally obtained values of **A**

and **D**. Because **A** and **D** are more fundamental measures of the seismic energy delivered to a given site than **M** and **LOG R**, in general **A-D** models should yield equivalent, or slightly superior performance, when compared with **M-LOG R** models. Unfortunately, our MLR database contains many estimated values of **A** and **D**, and the poorer quality of these data appears to be hampering our ability to develop satisfactory **A-D** models.

The LSI model proposed by Youd and Perkins (1987) and the site-specific models developed in the previous section suggest that a more comprehensive MLR model(s) for predicting ground displacement should include, but not be restricted to the following factors:

$$\text{LOG } D_H = f(M, \text{LOG R}, \text{LOG W}, \text{LOG S}, T_{15}, F_{15}, D50_{15}, N1_{60s}). \qquad (4.1.3)$$

In developing preliminary MLR models from this function, we divided the MLR database into two databases, one for free face failures and one for ground slope failures and attempted fitting separate regression coefficients for **M** and **LOG R** for each type of failure. However, this attempt yielded unsatisfactory results. We concluded that the U.S. database does not contain a sufficient number of ground slope failures to independently adjust the ground slope model for the effects of **M** and **LOG R**. To overcome this limitation, we combined the free face and ground slope databases and formulated the MLR model to fit common earthquake regression coefficients for each type of failure. The same model was formulated to fit separate topographical, geological, and soil parameters for free face and ground slope failures:

$$\text{LOG } D_H = f(M, \text{LOG R}, \text{LOG } W_{ff}, T_{15ff}, F_{15ff}, D50_{15ff}, N160_{ff}, \text{LOG } S_{gs}, T_{15gs}, F_{15gs}, D50_{15gs}) \qquad (4.1.4)$$

The subscripts **ff** and **gs** in Equation 4.1.4 indicate those variables that were assigned to the free face and ground slope components of the model, respectively. Inherent in this formulation is the assumption that **M** and **LOG R** influence free face failures in the same way that they influence ground slope failures. This appears to be a reasonable assumption because the amount of seismic energy delivered to a free face and a ground slope failure is the same for a particular seismic event and liquefaction locality. Given that we separately adjust each type of failure for the effects of topographical, geological and soil conditions (i.e., **W**, **S**, **T**, **F**, **D50**, and $\mathbf{N1_{60}}$), it seems reasonable to fit common earthquake parameters for free face and ground slope failures.

Based on the function expressed in Equation 4.1.4, we formulated the following MLR model:

$$\begin{aligned}\text{LOG}(D_H+0.01) = {} & b_0 + b_{0ff} + b_1 M + b_2 \text{LOG R} + b_3 \text{LOG } W_{ff} + b_4 T_{15ff} + b_5 F_{15ff} + b_6 D50_{15ff} \\ & + b_7 N1_{60ff} + b_8 \text{LOG } S_{gs} + b_9 T_{15gs} + b_{10} F_{15gs} + b_{11} D50_{15gs}\end{aligned} \qquad (4.1.5)$$

The fitted parameter $\mathbf{b_0}$ is the intercept of the combined free face and ground slope components of the model. The regression coefficient $\mathbf{b_{0ff}}$ is used to adjust $\mathbf{b_0}$ for any difference that may exist between the intercepts of the free face and ground slope components (i.e., the intercept for the free face component of the model is calculated by adding $\mathbf{b_0}$ and $\mathbf{b_{0ff}}$). Because log(0) is undefined, we expediently added 0.01 m to all values of $\mathbf{D_H}$ prior to performing the regression. This expediency enabled us to calculate log($\mathbf{D_H}$) for the zero displacement observations that are included in our MLR database.

A least squares fit of Equation 4.1.5 yields these regression coefficients: $\mathbf{b_0}$ = -5.085, $\mathbf{b_{0ff}}$ = -0.559, $\mathbf{b_1}$ = 0.976, $\mathbf{b_2}$ = -1.053, $\mathbf{b_3}$ = 0.693, $\mathbf{b_4}$ = 0.0272, $\mathbf{b_5}$ = -0.0328, $\mathbf{b_6}$ = -1.124, $\mathbf{b_7}$ = -0.0118, $\mathbf{b_8}$ = 0.356, $\mathbf{b_9}$ = 0.0403, $\mathbf{b_{10}}$ = -0.0336, $\mathbf{b_{11}}$ = -1.535. The $\mathbf{R^2}$ for this equation is 74.9 percent and all regression coefficients, except for $\mathbf{b_7}$, are significant at the 99 percent confidence level. The fitted value for $\mathbf{b_7}$ is significant at the 92 percent confidence level. Figure 4-1 shows that 89 percent (i.e., 399 out of 448) of the predicted displacement values fall

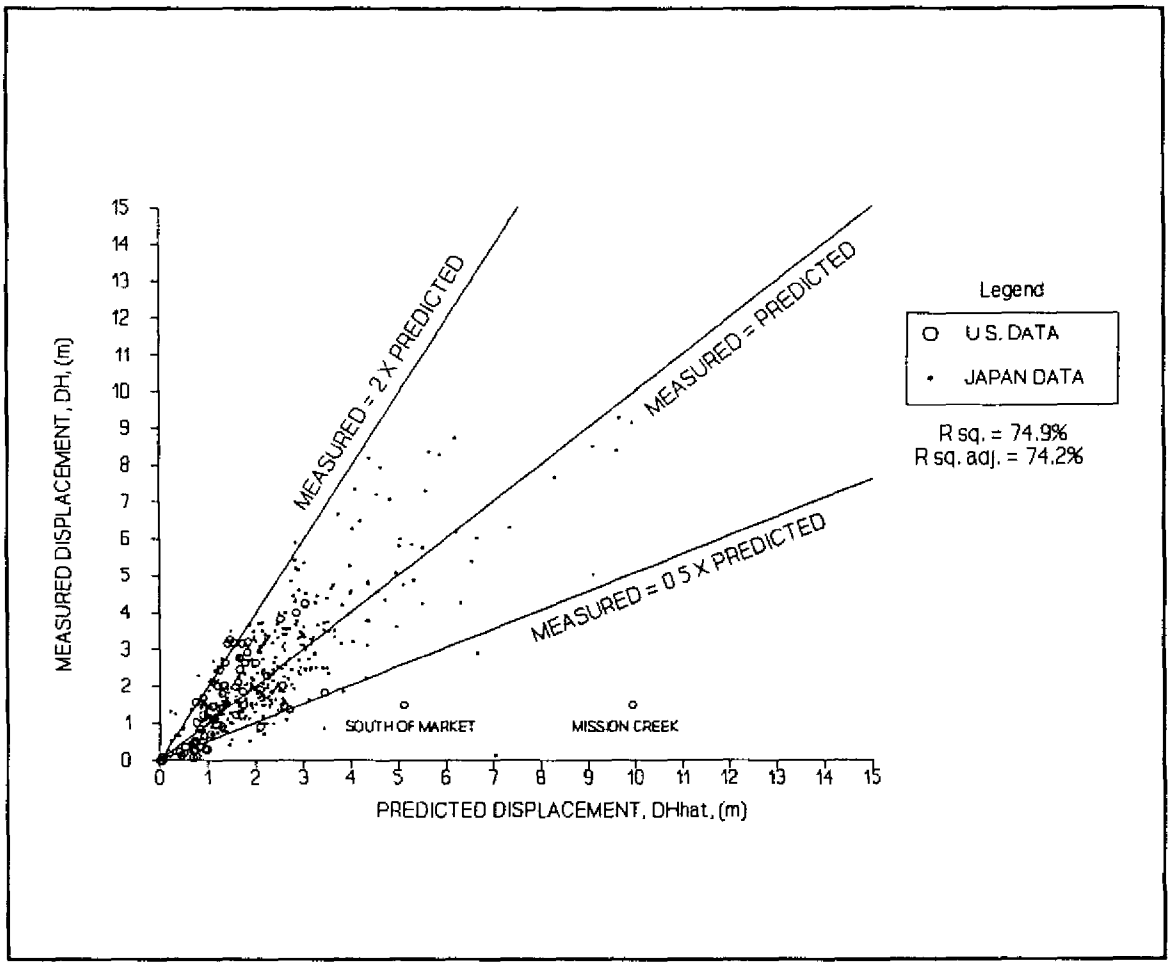

Figure 4-1 Plot of measured displacements, D_H, versus predicted displacements, D_{Hhat}, for model 4.1.5 using Japanese and U.S. case history data.

between the 100 percent overprediction and 50 percent underprediction bounds. The free face component of Equation 4.1.5 is:

$$\text{LOG}(D_H+0.01) = -5.644 + 0.976\,M - 1.053\,\text{LOG}\,R + 0.693\,\text{LOG}\,W + 0.0272\,T_{15} - 0.0328\,F_{15} - 1.124\,D50_{15} - 0.0118\,N1_{60s} \qquad (4.1.5a)$$

and the ground slope component is:

$$\text{LOG}(D_H+0.01) = -5.085 + 0.976\,M - 1.053\,\text{LOG}\,R + 0.356\,\text{LOG}\,S + 0.0403\,T_{15} - 0.0336\,F_{15} - 1.535\,D50_{15}. \qquad (4.1.5b)$$

Based on our data, Equation 4.1.5 appears to be performing reasonably well for M = 6.5 to 7.5 earthquakes and for liquefied sites within a 30 km radius of the seismic source. However, a comparison with data published by Ambraseys (1988) shows that Equation 4.1.5 will tend to overpredict D_H at liquefied sites with R > 30 km. In his study, Ambraseys compiled values of M_w and the farthest distance to observed liquefaction effects, R_f, (km), for several earthquakes and bounded these data with the equation:

$$M = 0.18 + 9.2 \times 10^{-5} R_f + 0.90 \text{ LOG } R_f. \qquad (4.1.6)$$

(See solid, curved bound shown on Figure 4-2). Ambraseys' study suggests that liquefaction (i.e., ground displacement, fissures, sand boils, etc.) are almost always located within this bound and for $R > R_f$, liquefaction effects are usually not observed. We used Equation 4.1.5 to back-calculate the distance, R, corresponding to the inception of lateral spread by using D_H = 0.05 m and mean values of W, S, T_{15}, F_{15}, $D50_{15}$, $N1_{60S}$ from our MLR database (Table 4-1). Figure 4-2 shows the results superimposed upon Ambraseys' data and R_f bound. This plot shows that the free face component of Equation 4.1.5 continues to predict ground displacement beyond Ambraseys' R_f bound beginning at M > 6.25 and R > 30 km and the ground slope component of Equation 4.1.5 does likewise for M > 7.0 and R > 70 km. Because Equation 4.1.5 does not correctly attenuate D_H with increasing R, we concluded that it should not be applied at sites with R > 30 km. This is a serious limitation to the application of Equation 4.1.5, especially for evaluating large earthquakes that typically produce significant lateral spread displacement beyond 30 km. Unfortunately, most of our case history sites are from R ≤ 30 km; thus, there is very limited information for adjusting Equation 4.1.5 based solely on our compiled data.

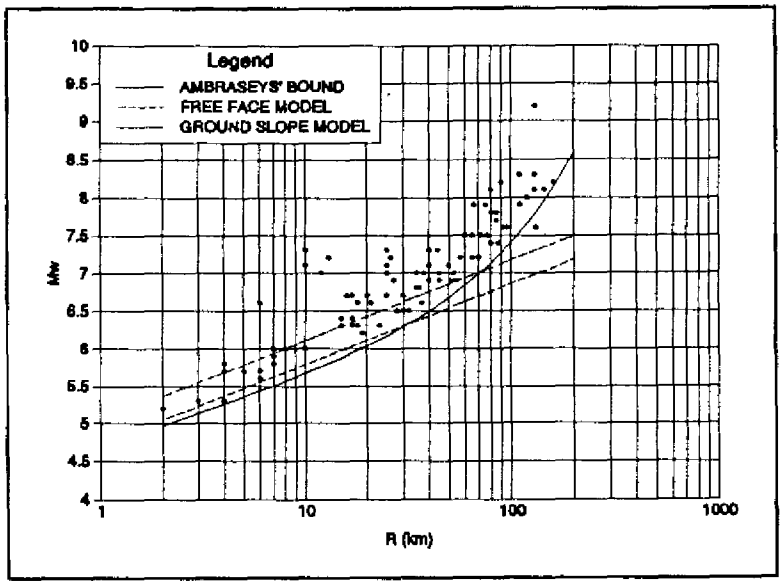

Figure 4-2 Performance of MLR model prior to including Ambraseys' data and adding a R term.

The data from Ambraseys' study, however, offer a means of adjusting Equation 4.1.5 so that it more properly attenuates LOG D_H as a function of R. To this end, we included 19 observations from Ambraseys' study (Table 4-2) in our analysis to strengthen the MLR database for R > 30 km. Because the majority of our case history sites are from earthquakes with 6.4 ≤ M ≤ 6.6 and 7.4 ≤ M ≤ 7.8, we selected only those observations from Ambraseys' study that fall within these same ranges. Also, prior to incorporating Ambraseys' data into the regression analysis, we needed reasonable estimates of the topographical, geological, and soil conditions at these sites. Because these factors were not compiled by Ambraseys, we decided to use average values of LOG W, LOG S, T_{15}, F_{15}, $D50_{15}$, $N1_{60S}$ from our database to approximate average site conditions at Ambraseys' sites (Table 4-1). In addition, because Ambraseys' sites represent the maximum R to observable liquefaction effects, we assumed that a minimal amount of lateral spread occurred at these localities and assigned D_H = 0.05 m to the observations listed in Table 4-2. Also, these observations were randomly assigned to either the free face or ground slope component of our MLR model prior to performing the regression analyses.

The functional form of Ambraseys' equation suggests that, in addition to the earthquake factors, M and LOG R, we need to include a R term in Equation 4.1.5. Therefore, we postulate that:

$$\text{LOG}(D_H+0.01) = b_0 + b_{0ff} + b_1 M + b_2 \text{LOG } R + b_3 R + b_4 \text{LOG } W_{ff} + b_5 T_{15ff} + b_6 F_{15ff} + b_7 D50_{15ff} + b_8 N1_{60Sff} + b_9 \text{LOG}(S)_{gs} + b_{10} T_{15gs} + b_{11} F_{15gs} + b_{12} D50_{15gs} \qquad (4.1.7)$$

A regression of this equation yields the following coefficients: b_0 = -6.086, b_{0ff} = -0.483, b_1 = 1.106, b_2 = -0.978, b_3 = -0.0101, b_4 = 0.703, b_5 = 0.0269, b_6 = -0.0308, b_7 = -0.983, b_8 = -0.0118, b_9 = 0.373, b_{10} = 0.0384, b_{11} = -0.0304, b_{12} = -1.096. All regression coefficients are significant at the 99 percent confidence level, except for b_8 which is only significant at the 93 percent confidence level, respectively. The R^2 for this equation is 83.6 percent.

Once again we used Equation 4.1.7 to back-calculate R for the inception of lateral spread by inputting D_H = 0.05 m and using the average site conditions listed in Table 4-1. Figure 4-3 shows the results compared with Ambraseys' data and R_f bound. The functional form of Equation 4.1.7 mimics Ambraseys' R_f bound quite well and the free face and ground slope components of the model provide a reasonable fit to Ambraseys' data. Thus, we concluded that the functional form of Equation 4.1.7 appears to more correctly attenuate D_H as a function of M and R than Equation 4.1.5.

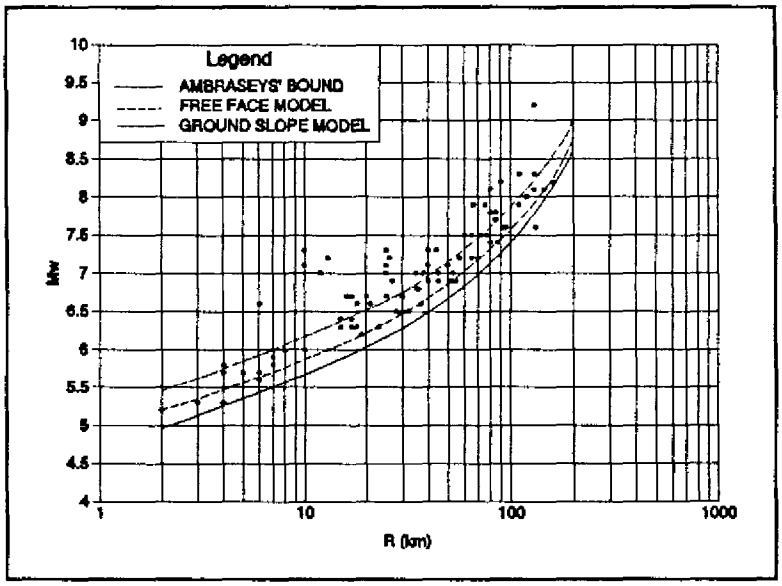

Figure 4-3 Performance of MLR model after including Ambraseys' data and adjusting for R.

A further examination of Equation 4.1.7 shows that $b_5 \approx b_{10}$, and $b_6 \approx b_{11}$, and $b_7 \approx b_{12}$, suggesting that common regression coefficients can be fitted for T_{15ff} and T_{15gs}, and for F_{15ff} and F_{15gs}, and for $D50_{15ff}$ and $D50_{15gs}$. Also, because the regression coefficient for $N1_{60ff}$, i.e., b_8, is significant only at the 93 percent confidence level, it was dropped from the analysis. Hence, we simplified the model to:

$$LOG(D_H+0.01) = b_0 + b_{0ff} + b_1 M + b_2 LOG R + b_3 R + b_4 LOG W_{ff} + b_5 LOG S_{gs} + b_6 T_{15} + b_7 F_{15} + b_8 D50_{15} \qquad (4.1.8)$$

After fitting Equation 4.1.8, we performed a sensitivity analysis and found that the transformation of T_{15} to **LOG** T_{15} and the transformation of F_{15} to **LOG** $(100-F_{15})$ yielded predicted displacements that are more credible for small values of T_{15} and F_{15}. Thus, we modified the model to:

$$LOG(D_H+0.01) = b_0 + b_{0ff} + b_1 M + b_2 LOG R + b_3 R + b_4 LOG W_{ff} + b_5 LOG S_{gs} + b_6 LOG T_{15} + b_7 LOG(100-F_{15}) + b_8 D50_{15} \qquad (4.1.9)$$

A least squares fit of Equation 4.1.9 yields the following regression coefficients: b_0 = -15.787, b_{0ff} = -0.579, b_1 = 1.178, b_2 = -0.927, b_3 = -0.013, b_4 = 0.657, b_5 = 0.429, b_6 = 0.348, b_7 = 4.527, b_8 = -0.922. All coefficients are significant at the 99.9 percent confidence level and the R^2 for Equation 4.1.9 is 82.6 percent. Figure 4-4 shows that 90 percent (421 out of 467) of the predicted displacement values, D_{Hhat}, fall between the 100 percent overprediction and 50 percent underprediction bounds. The free face component of Equation 4.1.9 is:

$$LOG(D_H+0.01) = -16.366 + 1.178 M - 0.927 LOG R - 0.013 R + 0.657 LOG W + 0.348 LOG T_{15} + 4.527 LOG(100-F_{15}) - 0.922 D50_{15} \qquad (4.1.9a)$$

and the ground slope component is:

$$LOG(D_H+0.01) = -15.787 + 1.178\,M - 0.927\,LOG\,R - 0.013\,R + 0.429\,LOG\,S + 0.348\,LOG\,T_{15} + 4.527\,LOG(100-F_{15}) - 0.922\,D50_{15} \quad (4.1.9b)$$

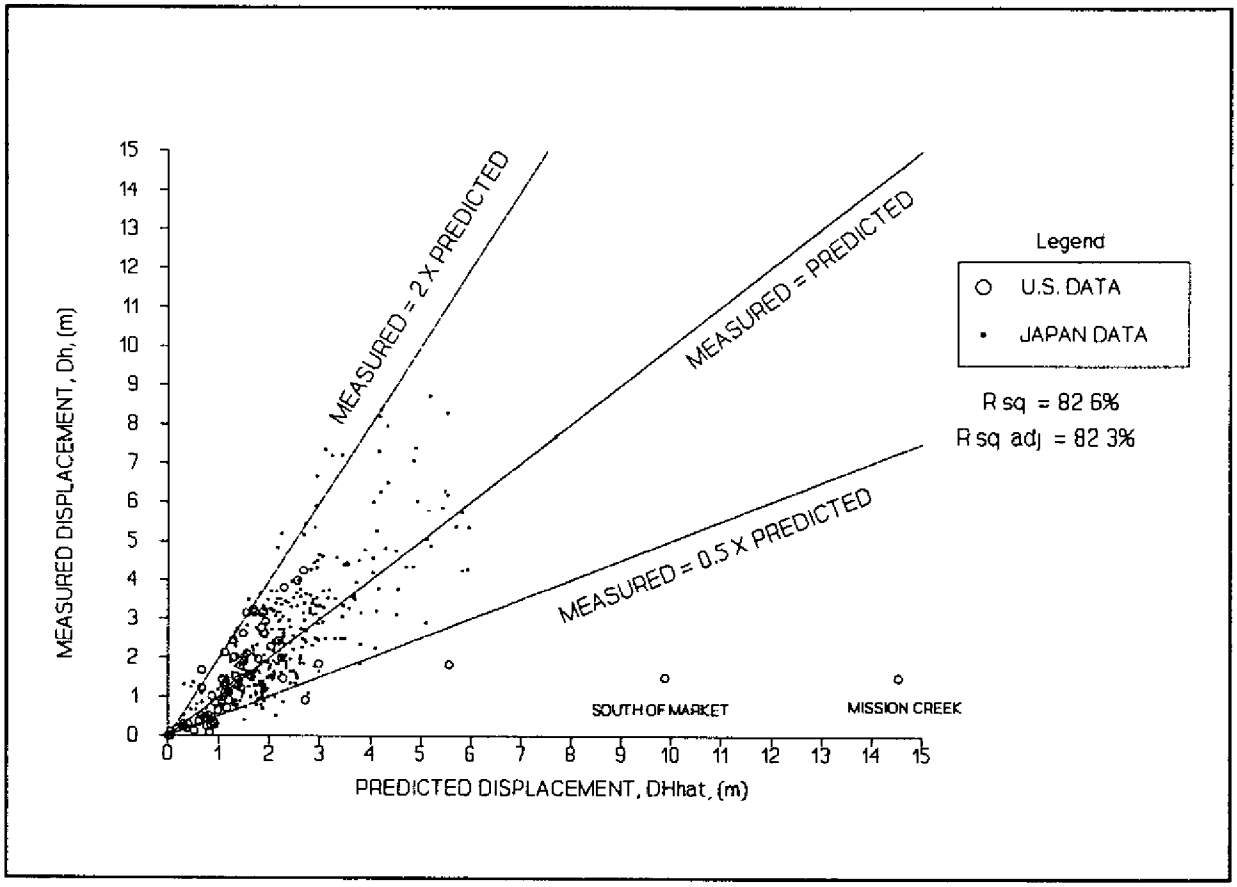

Figure 4-4 Plot of measured displacements, D_H, versus predicted displacements, D_{Hhat}, for Equation 4.1.9 using Japanese, U.S., and Ambraseys' data.

After fitting this model, we re-examined all independent variables listed in Table 3-2 for any linear trends that might greatly improve the performance of the model and found none. Thus, this is our final MLR model.

Although D_{Hhat} is an estimate of the average displacement, D_H, for a set of inputted **X(s)**, it is often desirable for engineering purposes to determine an upper bound or limit to the value of D_H that can be reasonably expected at a given site. Figure 4-4 shows that most values of D_{Hhat} predicted from the model fall below the "MEASURED = 2 X PREDICTED LINE." This suggests that if D_{Hhat} is increased by a factor of 2, then this result provides a conservative estimate of D_H that is not likely to be greatly exceeded. Also, because the relationship between D_H and the **X(s)** may be strongly nonlinear outside the ranges of the **X(s)** used in developing the model, extrapolation of Equation 4.1.9 may yield less reliable predictions. In short, it appears that this equation yields good results for $6.0 \le M \le 8.0$ earthquakes and at sites underlain by continuous layers of sands and silty sands having $N1_{60S} \le 15$; $0.075 \le D50_{15} \le 1.0$ mm, $0 \le F_{15} \le 50$ %, $1 \le T_{15} \le 15$ m, $Z_{BLS} \le 20$ m, $1 \le W \le 20$ %, and $0.1 \le S \le 6$ % (See Table 3-2 for definitions of these factors and Section 5 for a discussion of their

application.) Also, because this model was developed from Japanese and western U.S. data, it is most applicable to regions having high to moderate ground motion attenuation. Extrapolation of the model beyond these conditions may be warranted in some cases, if the inputted factors are reasonably close to these ranges and the extrapolation is deemed to yield conservative results (i.e., overly-predicted estimates of D_H). This model should not be applied to metastable soils (e.g., loess deposits, sensitive clays, and collapsible silts). These metastable soils were not analyzed by this study and may produce large ground displacements, or even flow failure.

TABLE 4-1
AVERAGE SITE CONDITIONS FOR CASE STUDIES TABULATED BY EARTHQUAKE

Earthquake	LOG W_f	LOG S_p	T_{15}	F_{15}[1]	$D50_{15}$[1]	$N1_{60f}$
1906 San Francisco	1.2981	-0.1549	4 6	18	0.227	6.4
1964 Alaska	1.3832	-1.0969	8.9	32	0.828	9.9
1964 Niigata	0.9244	-0.3188	9.5	10	0 311	4.8
1971 San Fernando	1.1427	0.0899	3 9	50	0.076	8.0
1979 Imperial Valley	0.8244	-0.2518	2 7	27	0.106	4.3
1983 Nihonkai-Chubu	——	0.1847	2.1	1	0.350	——
1987 Superstition Hills	1.3642	——	3.0	33	0.081	4.0
mean	**1.1562**	**-0.2580**	**5.0**	**24**	**0.283**	**6.2**

[1] The combined free face and ground slope data were used to calculate the means for T_{15}, F_{15}, and $D50_{15}$.

TABLE 4-2
OBSERVATIONS FROM AMBRASEYS' STUDY USED TO ADJUST MLR MODELS

M[1]	R[1]	LOG W_f	LOG S_p	T_{15}[2]	F_{15}[2]	$D50_{15}$[2]	$N1_{60f}$
7.8	80	1.1562	-------	5.0	24	0.283	6.2
7.5	77	——	-0.2580	5.0	24	0.283	——
6.5	28	1.1562	------	5.0	24	0.283	6.2
6.4	15	——	-0.2580	5.0	24	0.283	——
7.4	80	1.1562	——	5.0	24	0.283	6.2
6.6	18	——	-0.2580	5.0	24	0.283	——
7.6	92	1.1562	——	5.0	24	0.283	6.2
7.7	85	——	-0.2580	5.0	24	0.283	——
7.5	72	------	-0 2580	5.0	24	0.283	——
6.4	17	——	-0.2580	5.0	24	0.283	——
6.6	37	——	-0.2580	5.0	24	0.283	——
6.6	21	1.1562	——	5 0	24	0.283	6.2
6.5	30	1.1562	-------	5 0	24	0 283	6.2
7.5	65	——	-0.2580	5.0	24	0.283	—
6.5	32	1 1562	------	5.0	24	0.283	6.2
7.4	87	1 1562	——	5.0	24	0.283	6.2
7.5	60	——	-0.2580	5.0	24	0.283	—
7.8	85	——	-0.2580	5.0	24	0.283	—
7.6	95	1.1562	——	5.0	24	0 283	6.2

[1] **M** and **LOG R** values are from Ambraseys' case studies and values for **LOG** W_f, **LOG S**, T_{15}, F_{15}, $D50_{15}$, and $N1_{60}$ are averages from our MLR database (see Table 4-1).

[2] The same averages for T_{15}, F_{15}, and $D50_{15}$ were used in both the free face and ground slope components of the regression model.

SECTION 5
APPLICATION AND LIMITATIONS OF MLR MODEL

Figures 5-1 to 5-3 are histograms of the independent variables used in developing Equation 4.1.9. These graphs provide a general guide to the range of conditions for which this equation is applicable. This section further discusses the application and limitations of the MLR model.

5.1 Ground Motion Attenuation

Equation 4.1.9 was developed mainly from stiff-soil sites in the western U.S. and from stiff soil sites in Japan that were within 30 km of the seismic source. For these regions and conditions, Equation 4.1.9 should be directly applied to predict lateral spread displacement. For other regions of the world, such as the eastern U.S. where ground motion attenuates more slowly with distance, and for other site conditions, such as liquefiable deposits over soft clay layers where ground motion may be strongly amplified (i.e. soft soil sites), a correction must be applied to Equation 4.1.9 to account for these different seismic and site conditions. The preferred method to adjust the model would be to directly regress D_H on the earthquake factors, **M** and **A**. However, because **A** was measured only at a few of the case history sites, the direct development of a **M-A** model was not possible with the limited data. We attempted to estimate **A** from empirical **M-R** relationships (Appendix 1, Section A1.1.3) and use these estimates to develop a **M-A** model, but this attempt yielded poorer results than models based on **M**, **LOG R**, and **R**.

Until better case histories are assembled to adequately develop **M-A** and **A-D** models, we propose the following procedure to adjust the values of **R** that are used into Equation 4.1.9 for other regions of the world or for soft soil sites. Figure 5-4 is a plot of **A** estimated for stiff soil sites in the western U.S. using attenuation relationships and soil amplification factors published by Idriss (Idriss, in press; Idriss, 1990; Equation A1.1.3.2). These accelerations should roughly represent those incurred at our case history sites, which are primarily from stiff soil sites in the western U.S. and Japanese sites found within 30 km of the seismic source. The values of **A** plotted on this figure were calculated for their respective values of **M** and **R** by applying a peak-acceleration attenuation equation developed by Idriss for bedrock sites and then correcting those bedrock accelerations for stiff soil conditions. To adjust the bedrock accelerations to stiff soil conditions, we multiplied the peak bedrock accelerations by a correction factor that was estimated from an acceleration amplification curve for soft soils published by Idriss (1990) (Figure 5-5). The stiff soil acceleration curve was approximated by fitting a series of points that were positioned midway between the non-amplification curve for rock (i.e., 45 degree line) and the high-amplification curve for soft soils (Figure 5-5). The procedure for using the curves shown in Figure 5-4 to correct the **R** inputted into Equation 4.1.9 for soft soil sites or non-western U.S. or non-Japanese sites is as follows. (1) Using standard procedures, the design earthquake magnitude, **M**, and peak ground acceleration, **A**, are determined for the candidate site. (2) That magnitude and acceleration are then plotted on Figure 5-4. (3) From that plotted point, an equivalent source distance, R_{eq}, is interpolated from the R-curves given in Figure 5-4. (4) That R_{eq} is then entered into Equation 4.1.9 instead of the actual R to calculate D_H. For example, during the 1989 Loma Prieta, California earthquake (M_w = 6.9), liquefaction and minor lateral spreading occurred on Treasure Island, at a distance of about 80 km from the seismic energy source. Application of that distance in Equation 4.1.9 along with appropriate site properties indicates that an insignificant amount of displacement should have occurred on the island. (This site also falls outside of Ambraseys' R_f bound, suggesting that liquefaction should have not occurred.) However, considerable ground motion amplification was measured at Treasure Island, which was constructed by placing hydraulic fill over thick deposits of soft, San Francisco Bay mud.

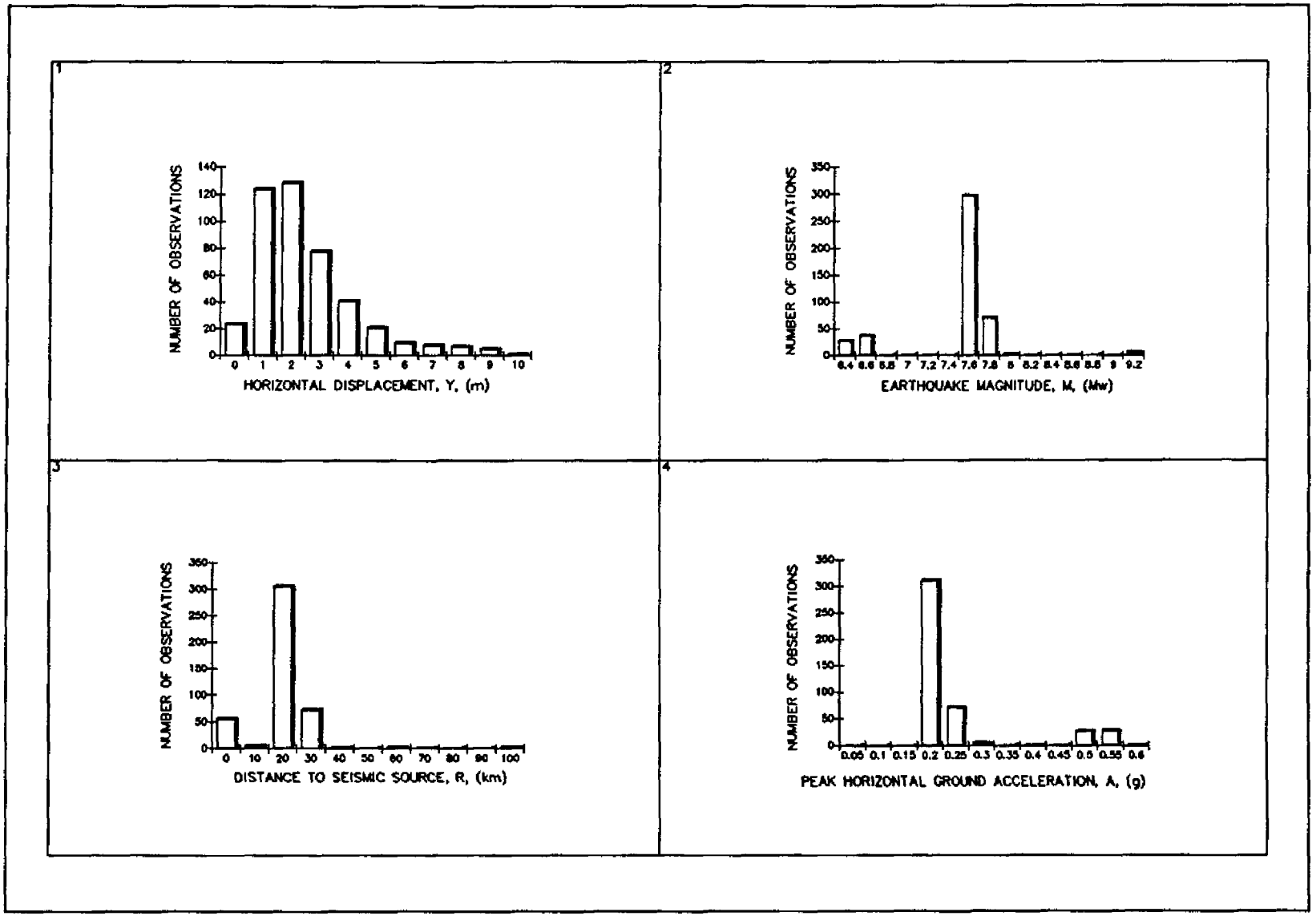

Figure 5-1 Histograms for (1) displacement, D_H, (2) magnitude, M, (3) distance to seismic energy source, R, (4) peak ground acceleration, A.

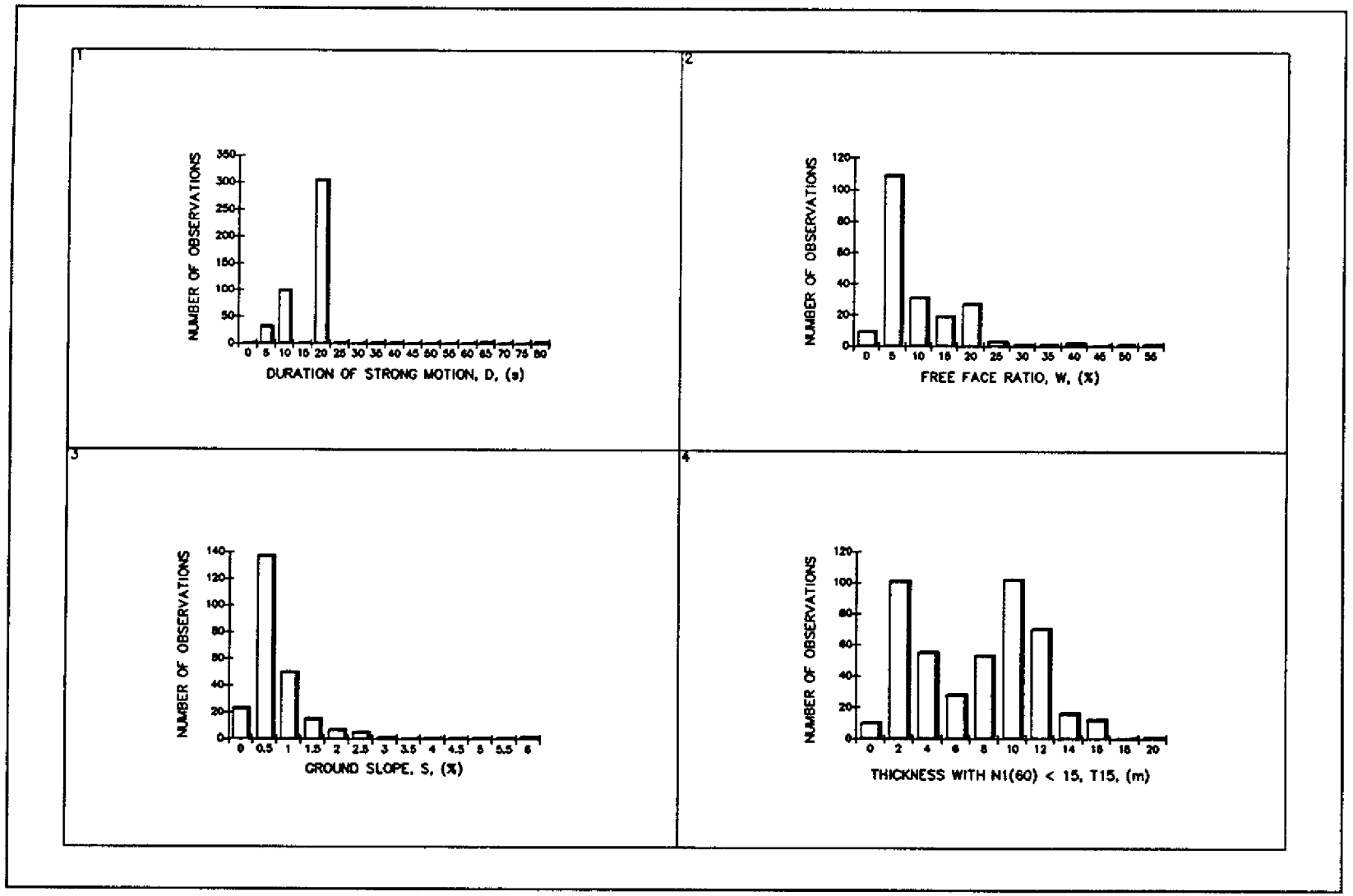

Figure 5-2 Histograms for (1) duration, D, (2) free face ratio, W, (3) ground slope, S, and, (4) thickness with $(N1)_{60} < 15$, T_{15}.

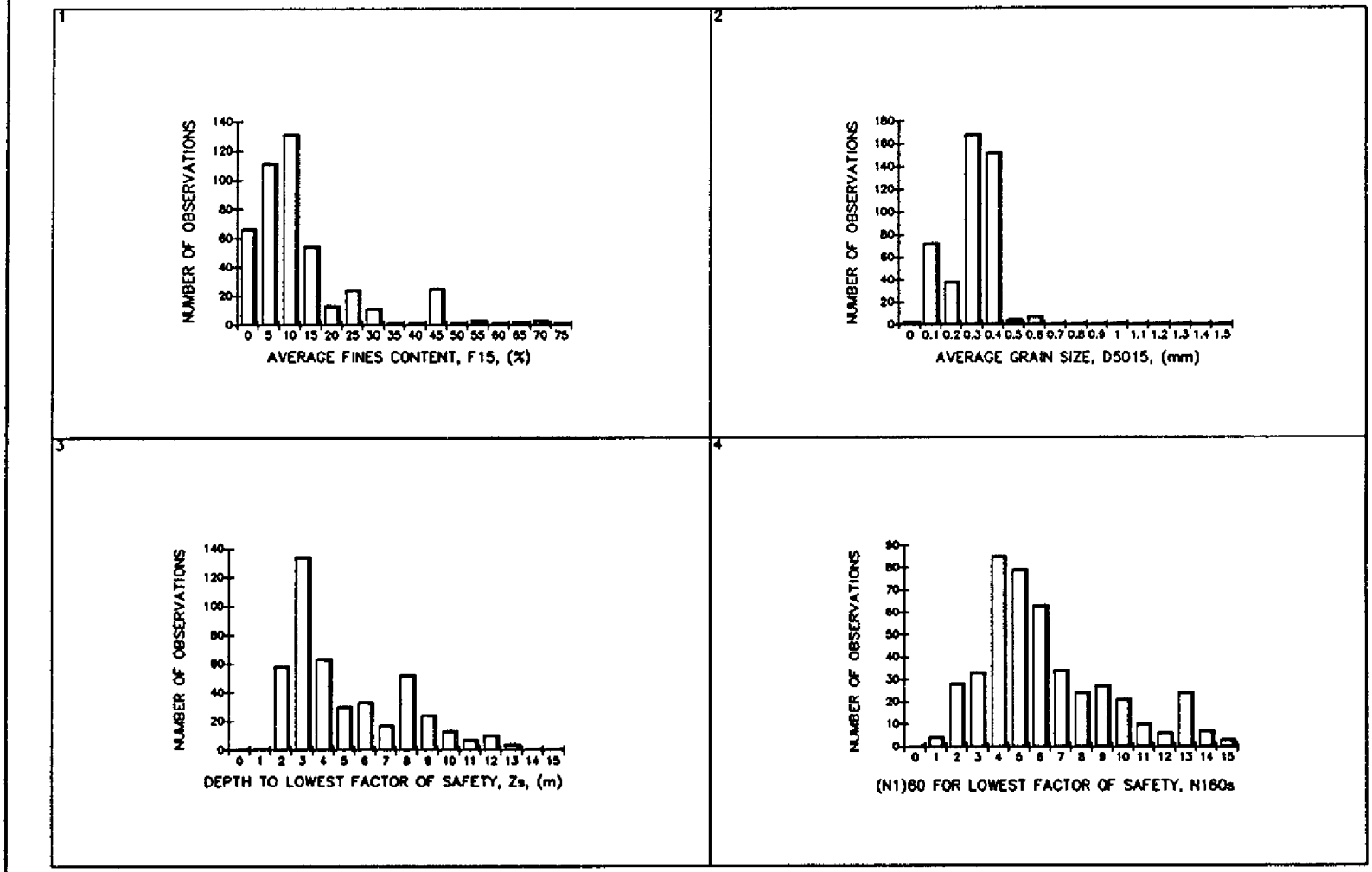

Figure 5-3 Histograms for (1) fines content, F_{15}, (2) mean grain size, $D50_{15}$, (3) depth to low FS, Z_s, (4) lowest $N1_{60s}$.

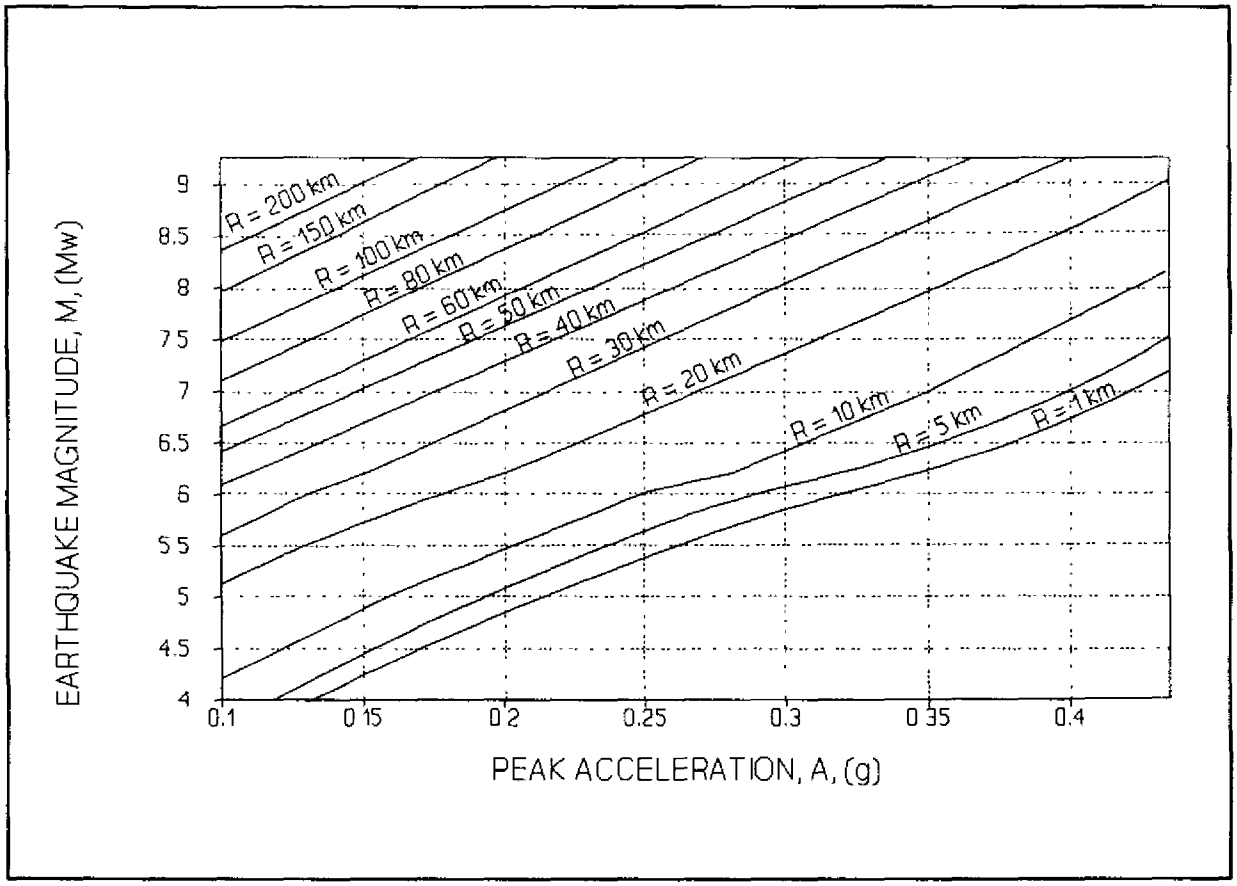

Figure 5-4 Graph for Determining Equivalent Source Distance, R_{eq}, from Magnitude and Peak Acceleration.

Although maximum bedrock accelerations measured just a few hundred meters away on nearby Yerba Buena Island were roughly 0.07 g, and accelerations measured on nearby stiff soil sites were generally about 0.10 g, the instrumented value of **A** on Treasure Island was 0.16 g. Thus, this measured **A** was more than twice the bedrock acceleration and was also significantly higher than that expected for stiff soil sites at that distance. However, if **M** = 6.9 and **A** = 0.16 is plotted on Figure 5-4, the resulting R_{eq} is about 50 km (compared to the actual source distance of 80 km). Entering a R_{eq} of 50 km into Equation 4.1.9 with the appropriate soil properties predicts that a few tenths of a meter of lateral spread displacement should occur near the free face edges of the island. This prediction roughly corresponds with that measured on Treasure Island after the earthquake.

5.2 Earthquake Magnitude

The bulk of our data are from $6 \leq M \leq 8$ earthquakes and extrapolation of Equation 4.1.9 beyond this range increases the uncertainty in the predicted displacements (Figure 5-1). However, because lateral spread displacement appears to decrease markedly for $M < 6$ earthquakes, extrapolation of Equation 4.1.9 to $M < 6$ earthquakes appears to yield predicted displacements, which with conservative allowance for the greater uncertainty, appear to be usable for engineering analyses. Extrapolation of the equation to earthquakes with $M > 8$ also appears to give reasonable predictions for fine to coarse grain sands and silty sands based on the limited data available from extremely large earthquakes. (Seven

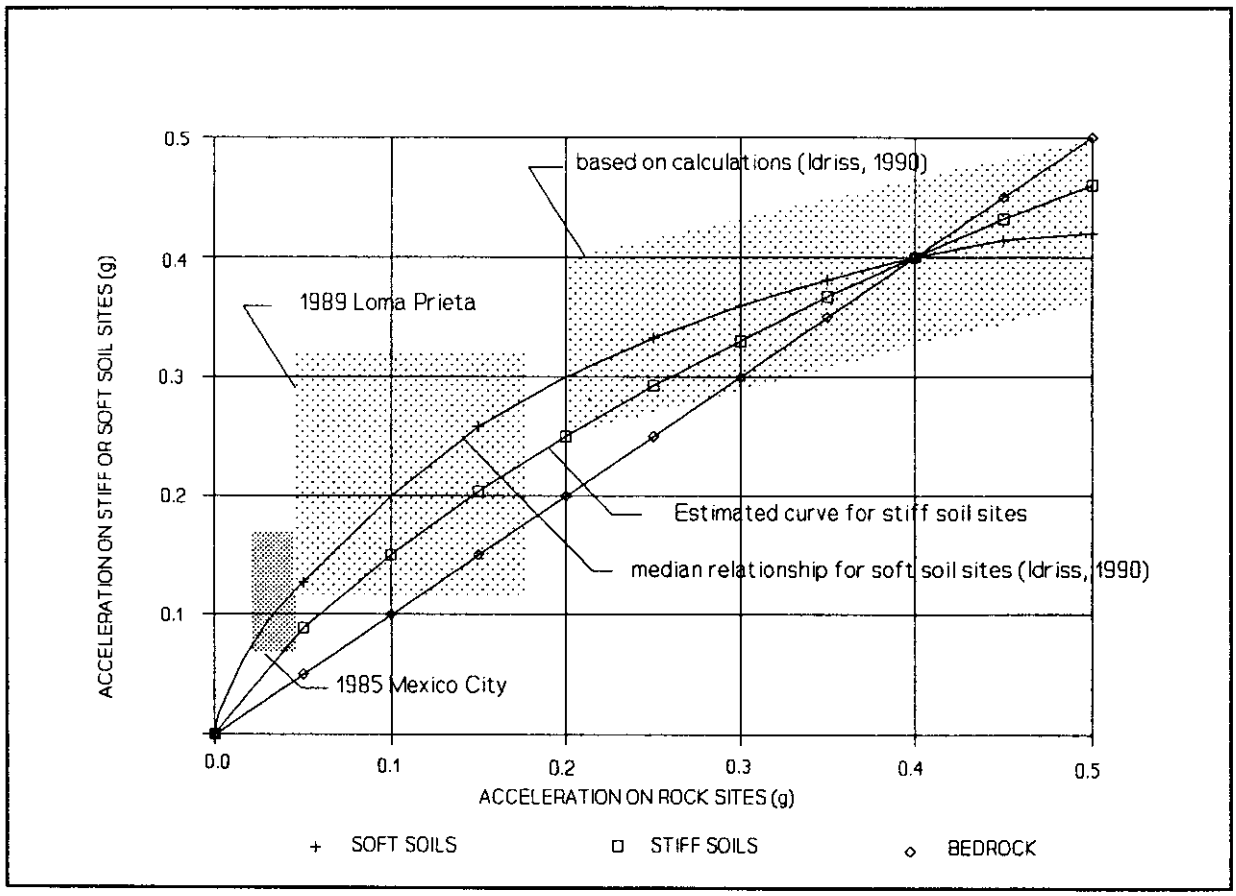

Figure 5-5 Approximate Curve for Estimating A for Stiff Soil Sites (Modified from Idriss, 1990).

observations from the 1964 Alaska earthquake (**M** = 9.2) were fitted and an examination of the $\varepsilon_s(s)$ for these data shows no unusual residual behavior (see $\varepsilon_s(s)$ versus **M** plot in Appendix 2 for Equation 4.1.9).) Nonetheless, the addition of more case studies for **M** > 8 earthquakes would strengthen the MLR database and improve its reliability for extremely large events.

5.3 Distance to the Fault Rupture or Zone of Seismic Energy Release

Equation 4.1.9 appears to attenuate D_H with increasing **R** in a manner that is consistent with our case history data and with Ambraseys' R_f bound. On the other hand, if the inputted **R** is allowed to decrease to a distance that is approaching zero, the predicted displacements from Equation 4.1.9 can become quite large, especially for **M** > 7.5. Based on a sensitivity analysis, in which we allowed **M** to vary from 6.5 to 9.5 and using the average site conditions given in Table 4-1, we noted that D_{Hhat} becomes unreasonably large (e.g., larger than 5 to 10 m) when the inputted **R** is allowed to decrease below the values listed in Table 5-1. Because Equation 4.1.9 appears to yield predicted displacements that are larger than those normally expected for lateral spread and because only a few case histories are available for lateral spreads located very near the seismic source, extrapolation of Equation 4.1.9 to distances less than those listed in Table 5-1 may yield unreliable estimates of D_H.

TABLE 5-1
MINIMUM VALUES OF R FOR VARIOUS EARTHQUAKE MAGNITUDES

M	R (km)
6.5	0.25
7.0	1
7.5	5
8.0	10
8.5	25
9.0	50

5.4 Free Face Ratio and Ground Slope

Most of the free face failures analyzed by this study are for W ≤ 20 percent and caution should be used when extrapolating the MLR model beyond this value. However, some extrapolation may be warranted at sites where the liquefiable sediments are not deemed to be prone to slumping or flow failure. For example, an important problem for engineers is the estimation of the potential lateral spread displacement near bridge crossings where W typically exceeds 20 percent. In this study, six observations having 20 < W ≤ 55 percent were fitted and Equation 4.1.9a appears to yield credible predictions for this range. Nonetheless, field observations of free face failures along river channels reveals that the displacement may have a significant vertical component due to rotation of slump blocks. Also, gravitational shear forces near the free face may be large enough to induce flow failure in highly susceptible soils. If slumping or flow failure is a potential concern, Equation 4.1.9 is not applicable and more sophisticated 2-D models, such as dynamic, finite-element analyses should be used (Prevost, 1981; Finn and Yogendrakumar, 1989).

In formulating Equation 4.1.9a, we attempted a MLR model that included both W and S as topographical factors, but our analyses suggested that the inclusion of S does not significantly improve the performance of the free face model. Thus, we concluded that the slope of the river banks, either into or away from the channel, does not vary enough to have markedly affect displacement when compared with the influence exerted by W. However, most of the free face failures in our database had values of S < 0.5 percent. If additional conservatism is desired at sites where S > 0.5 percent, the results from the ground slope component, (i.e., Equation 4.1.9b) could be added to the results of the free face component, (i.e., Equation 4.1.9a); but in most cases, we do not believe that this degree of conservatism is required.

In applying Equation 4.1.9 to sites which are farther removed from the free face, questions may arise about whether to apply Equation 4.1.9a or Equation 4.1.9b. In highly liquefiable sediments, like those found in Niigata, movement of the river banks towards the channel initiated at a maximum distance of 100 times the height of the channel (i.e., 100 H). Thus, in highly susceptible soils, the free face appears to influence D_H for values of W ≥ 1 percent. (Note that 100 H is equal to a W value of 1 percent). However, we do not recommend the exclusive use of the Equation 4.1.9a at all sites with W ≥ 1 percent. Figure 3-4 shows that at some places in Niigata, free face failure was not initiated until W was about 5 percent. Thus, for sites with 1 ≤ W ≤ 5 percent, it is possible that D_H may be also influenced by S, and the ground slope model may be just as applicable as the free face model. For ambiguous cases, we suggest estimating D_H from both Equation 4.1.9a and 4.1.9b and applying the larger value for design purposes. As previously mentioned, if the designer believes that both the free face and ground slope will contribute to produce displacement, then both components of Equation 4.1.9 could be added to produce a conservative estimate of D_H.

For the ground slope failures evaluated herein, **S** ranged from about 0.1 percent to 6 percent. Extrapolation of Equation 4.1.9b beyond this range may lead to uncertain predictions. For **S** < 0.1 percent, chaotic displacements due to ground oscillation are likely to exceed those from lateral spreading and Equation 4.1.9b may give uncertain estimates of D_H for flat ground conditions. Also, ground slopes that exceed 6 percent may cause flow failure in highly susceptible soils and consequently produce large displacements. Equation 4.1.9b is not valid for estimating D_H for such conditions.

5.5 Gravelly Soils

During preliminary analyses, we noted that our MLR models performed poorly at predicting lateral spread displacements measured at gravelly sites from the 1964 Alaska and 1983 Borah Peak, Idaho earthquakes. Due to the high number of outliers for gravelly sites, it appears that gravel has a different displacement behavior than sand and silty sand. For example, Figure 5-6 shows the $e_s(s)$ plotted against $D50_{15}$ for one of our preliminary MLR models. Four of 6 observations with $D50_{15}$ values > 2 mm are potential outliers. These outliers are from alluvial gravels that underwent lateral spread at Whiskey Spring and Pence Ranch during the 1983 Borah Peak, Idaho, earthquake (Andrus and Youd, 1987).

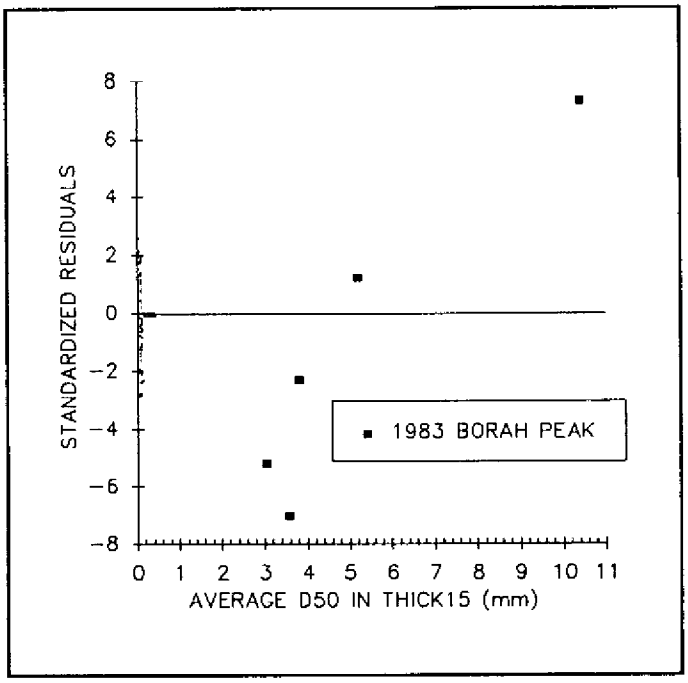

Figure 5-6 Standardized residuals, e_s's, plotted against the average mean grain size, $D50_{15}$, in T_{15}, showing outliers in gravelly soils.

Because our data contains only a few examples of lateral spread at gravelly sites, we did not have an adequate number of observations to properly fit the displacement behavior of gravelly sediments. Thus, we removed observations with $D50_{15}$ > 2 mm from the MLR database prior to fitting Equation 4.1.9. (Case histories at Whiskey Springs, Idaho; Pence Ranch, Idaho; and some gravelly sites in Alaska were removed). Figure 5-6 also shows that there are very few observations for 1 < $D50_{15}$ ≤ 2 mm. Consequently, for verified predictions, we restrict the use of Equation 4.1.9 to saturated cohesionless sediments with $D50_{15}$ values ≤ 1 mm.

5.6 Fines Content and Layered Profiles

In addition to $D50_{15}$, there are limits on the range of the average fines content, F_{15}, for which Equation 4.1.9 has been verified. Figure 5-3 shows that most of F_{15} values in the MLR database are from soils with F_{15} values ≤ 50 percent; thus, we limit the use of Equation 4.1.9 to this range. Also, because F_{15} is strongly correlated with $D50_{15}$, there are limits on the allowable range for the combination of these factors. Figure 5-7 is a plot of F_{15} versus $D50_{15}$ for the 267 boreholes included in this study. This plot shows the envelope of F_{15} and $D50_{15}$ values for which Equation 4.1.9 has been verified. Extrapolation of the model to soils with textures beyond these limits introduces extra uncertainty into the predicted displacement.

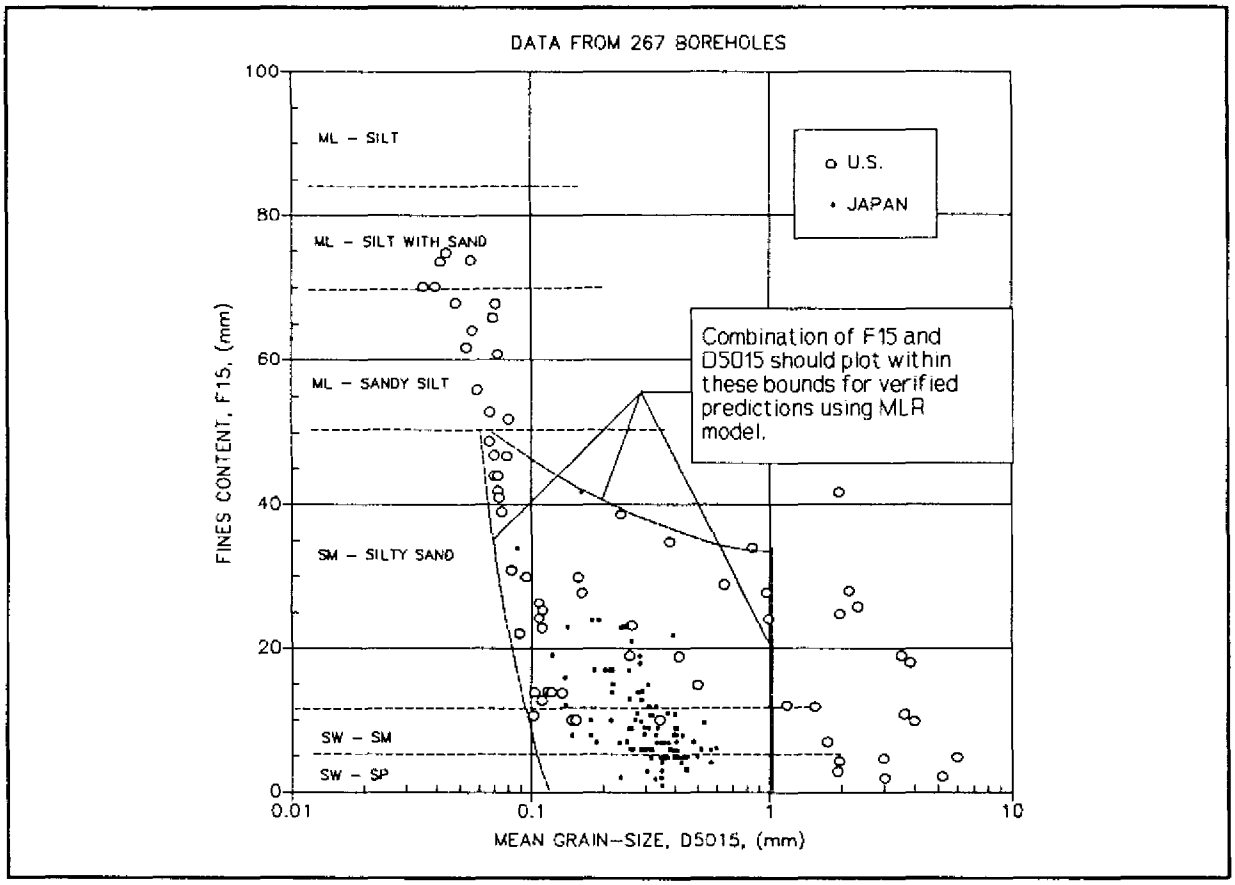

Figure 5-7 Plot of ranges of F15 versus $D50_{15}$ for which Equation 4.1.9 has been verified (data from 267 boreholes).

Equation 4.1.9 suggests that fines content has a major influence on lateral spread displacement. All other factors remaining constant, predicted displacements diminish rapidly with increasing fines content. For example, lateral spread at Juvenile Hall during the 1971 San Fernando Valley, California earthquake illustrates the marked affect that the inputted fines content has on predicted values of displacement. Lateral spread at Juvenile Hall ranged from 0.5 to 1.68 m and occurred on a gentle ground slope (S = 1.2 %) (Bennett et al., 1989; Youd, 1973b). Liquefaction appears to have occurred primarily in a sandy silt (ML) layer that is interbedded with thinner, silty sand (SM) layers. The T_{15} layer at Juvenile Hall has an average fines content of about 59 percent and an average mean grain size of 0.06 mm. Equation 4.1.9 predicts a maximum displacement of about 0.7 m for Juvenile Hall, which underestimates the maximum observed value by a factor slightly greater than 2 (Figure 5-8). However, further examination of the borehole data and watertable elevations taken soon after the earthquake suggests that a relatively thin, continuous silty sand (SM) layer may have liquefied just below the watertable. If this SM layer is analyzed separately, and not averaged with the thicker, underlying ML layer, the inputted factors are: T_{15} = 0.6 m, F_{15} = 41 %, $D50_{15}$ = 0.131 mm and Equation 4.1.9b predicts an average displacement of about 1.8 m for this soil, which is in good agreement with the observed displacement. Thus, in analyzing a layered system with two potentially liquefiable layers that have distinctly different textures, averaging F_{15} and $D50_{15}$ throughout the entire T_{15} layer may produce smaller predicted displacements than if the individual layers are analyzed separately. This is especially true if the thickest layer has a high fines content. Hence, for

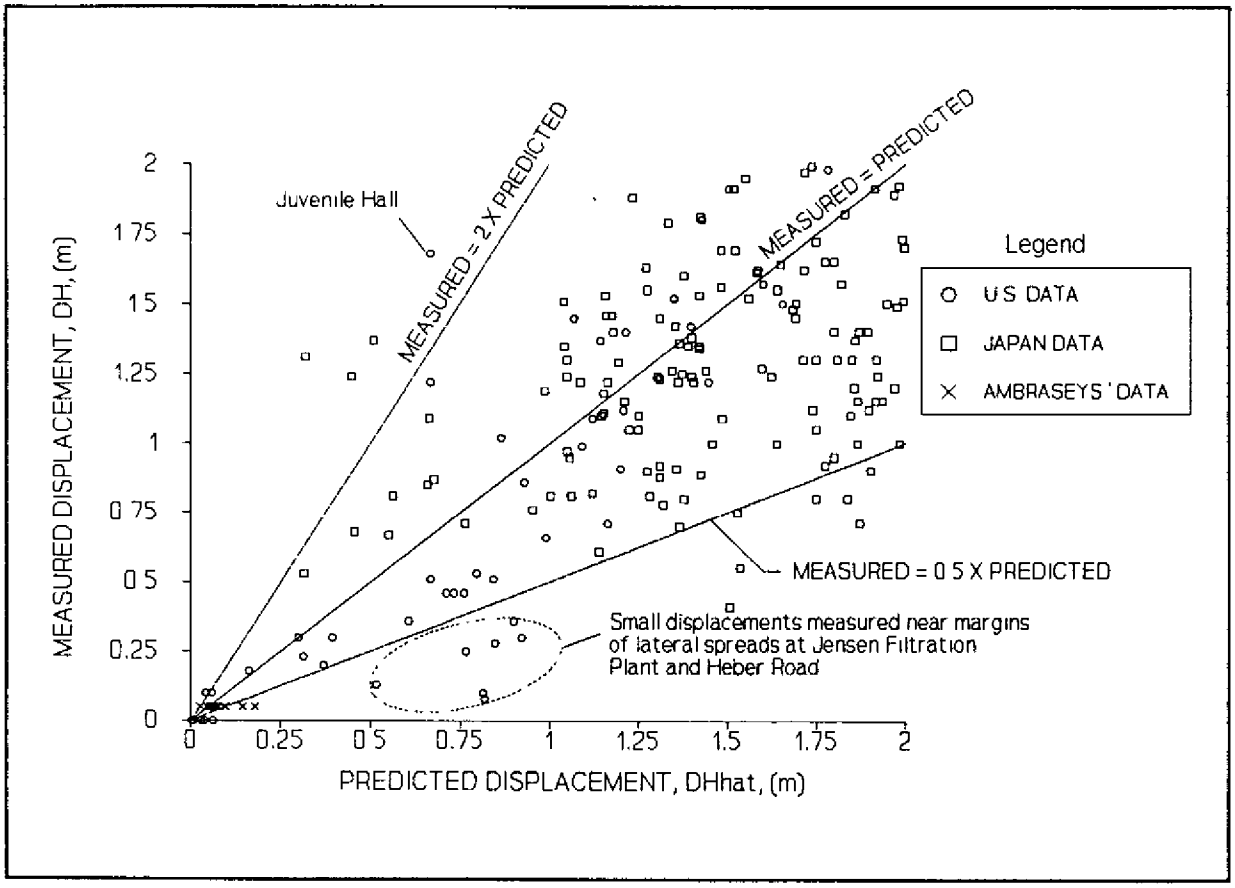

Figure 5-8 Plot of measured displacements versus displacements predicted by Equation 4.1.9 for displacements that are less than 2 meters.

conservative design in layered profiles, we recommend that distinctly different T_{15} layers be analyzed separately by calculating T_{15}, F_{15}, and $D50_{15}$ for each distinct soil type. The total predicted displacement may then be conservatively estimated as the sum of the displacements predicted for the individual layers. However, to divide the profile into individual layers, there must be a distinct textural difference between the layers.

Also, Figure 5-8 shows that a small number of Japanese observations are underpredicted by a factor greater than 2. The poorer quality of the subsurface data available for these observation or errors in the measured displacements at these locales (Section 3.2) may be the reason for the slight underprediction of these smaller displacements.

5.7 Soils with $(N1)_{60}$ Values Greater than 15

In almost all cases reviewed herein, significant ground displacement was restricted to saturated cohesionless soils having $(N1)_{60}$ values ≤ 15. This finding does not appear to be coincidental, nor does it appear to represent a deficiency in our MLR database. The case studies reviewed herein do include boreholes where all $(N1)_{60}$ values in the profile exceed 15 (e.g., boreholes from Juvenile Hall, Heber Road, Niigata, and Noshiro, Japan), but these boreholes were generally located near the margins of the lateral spreads where no appreciable amount of displacement was reported. Thus, in general, cohesionless materials with $(N1)_{60}$ values > 15 appear to be resistant to lateral spread displacement for

$M < 8$ earthquakes and we limit the application of Equation 4.1.9 to saturated, cohesionless soils having $(N1)_{60}$ values ≤ 15.

However, it is possible during the 1964 Alaska earthquake that fluvial deposits with $(N1)_{60}$ values > 15 underwent lateral spread. During this extremely large and long-lived earthquake ($M = 9.2$), gravelly, channel deposits ($15 \leq (N1)_{60} \leq 20$) displaced a maximum of 1 m at the Resurrection River and Placer Rivers (Bartlett and Youd, 1992). However, the quality of the subsurface data for these Alaskan sites is poor. The penetration tests at the Resurrection River were performed with a non-standard hammer and have questionable validity. Also, N values recorded in gravelly soils generally tend to be higher when compared with finer grained sediments of comparable relative densities. Thus, we found no conclusive evidence of significant displacement in sediments with $(N1)_{60}$ values > 15 for M > 8 earthquakes.

5.8 Thickness and Depth of the Liquefiable Layer

Prior to applying Equation 4.1.9, however, standard liquefaction analyses (Seed and Idriss, 1971; Seed et al., 1983; 1985; NRC, 1985) should be performed to verify that liquefaction is expected in the layer for the inputted earthquake factors (Figure 5-9). Based on the compiled case history data, it appears that lateral spread occurs in relatively thick, T_{15} layers (T_{15} values for our database average 5.5 m (Table 4-1)). In general, T_{15} is thicker than 1 m at locales that underwent a significant amount of lateral spread. In a few instances, however, small displacements occurred along the margins of some lateral spreads where the thickness of the T_{15} layer appears to be less than 1 m. Thus, for conservative design, we suggest that continuous, T_{15} layers having a thickness less than 1 m be considered as potential candidates for lateral spread. However, because our MLR database contains only a few cases of $T_{15} < 1$ m, Equation 4.1.9 may yield less reliable results for these conditions. Equation 4.1.9 should not be applied at sites having thin, noncontinuous, T_{15} layers. The researched database is deficient for such conditions.

Our liquefaction analyses also suggest that the depth to the top of the liquefied layer, Z_{TLS}, is usually found within the upper 10 m of the profile and that the depth to the bottom of the liquefied layer, Z_{BLS}, is usually found within the upper 20 m of profile at sites that underwent a significant amount of lateral spread. These same analyses also suggest that the depth to the lowest factor of safety against liquefaction, Z_S, generally occurs in the upper 15 m of the profile.

5.9 Residual Strength and SPT N Measures

Many analytical and numerical models use residual strength as a key input parameter for estimating liquefaction-induced ground displacement. Seed et al. (1988) have proposed an empirical curve relating residual strength with SPT $(N1)_{60}$ values. In this study, we also postulated that lateral spread is a function of residual strength and devised several SPT N and $(N1)_{60}$ variables to represent residual strength in our preliminary MLR models. We tested models that included the lowest N, lowest $(N1)_{60}$, average N, and average $(N1)_{60}$ values in the liquefied profile. Of these measures, $N1_{60S}$ (defined in Table 3-2) yielded the best results when included in the free face model developed for Niigata and Noshiro, Japan. (R^2 values for the models increased from 2 to 9 percent depending upon which other independent variables were present.) However, as the U.S. data were added to the analyses, $N1_{60S}$ made only a slight contribution to improving R^2 (R^2 increased only 0.1 percent when $N1_{60S}$ was present in the final model). Thus, this variable was dropped from the final model.

Given that lateral displacement is correlated with residual strength and that residual strength is a function of the lowest and average SPT N and $(N1)_{60}$ values in the liquefied profile, we offer the following explanations to why our SPT N

and $(N1)_{60}$ variables appear to be only modestly correlated with displacement. First, there probably is a certain amount of variability in the SPT N and $(N1)_{60}$ values tabulated in our MLR database due to the different types of hammers that were employed at the various case history sites. Second, perhaps the lowest and average N and $(N1)_{60}$ values in the MLR database do not vary enough to show a strong correlation with displacement. Tabulated values of $\mathbf{N1_{60S}}$ range from 1.3 to 14.7, and have a mean of 6.1 (Figure 5-3). Approximately 75 percent of the compiled $\mathbf{N1_{60S}}$ values are $\leq$ 8, and 90 percent are $\leq$ 10. Third, and most importantly, it appears that residual strength, and ground displacement are not solely a function of the lowest or average N and $(N1)_{60}$ values in the liquefied profile, but are strongly influenced by other subsurface and soil factors, such as the fines content, thickness, and mean-grain size of the liquefied layer. This study indicates that $\mathbf{F_{15}}$, $\mathbf{T_{15}}$, and $\mathbf{D50_{15}}$ are strongly to moderately correlated with displacement. Also, $\mathbf{T_{15}}$ correlates reasonably well with $\mathbf{N1_{60S}}$ ($R = -0.59$) suggesting that thick, $\mathbf{T_{15}}$ layers tend to have lower $\mathbf{N1_{60S}}$ values. Hence, we suggest that relatively thick, clean, fine-grained, $\mathbf{T_{15}}$ layers appear to produce lower residual strengths and are consequently subjected to a larger amount of ground displacement.

5.10 Boundary Effects

Because the regression coefficients for Equation 4.1.9 are heavily dependent upon Japanese case studies, where liquefaction was widespread and lateral boundary effects were relatively minor, our model may overpredict ground displacements occurring near the margins of smaller lateral spreads. Figure 5-8 shows that a few of the U.S. and Japan observations are overpredicted by a factor greater than 2. Overpredicted observations at the Jensen Filtration Plant and Heber Road were measured at the head or along the side margins of the lateral spreads where ground was apparently inhibited by the nearby lateral boundary. We suspect that changes in the subsurface geology played a large role in limiting liquefaction and ground displacement at these locales. Also, errors the estimates of $\mathbf{D_H}$ for these smaller displacements may have contributed to the underpredictions (Section 3.2).

Equation 4.1.9 also significantly overestimates ground displacement measured at Mission Creek and the South of Market Zone following the 1906 San Francisco earthquake (Figure 4-4). At these sites approximately 1.5 m of lateral spread occurred on gentle slopes of 0.6 to 0.8 percent, respectively (Youd and Hoose, 1978; O'Rourke et al., 1991). Equation 4.1.9 predicts approximately 7.5 m of displacement for the South of Market Zone and 12 m for the Mission Creek Zone. We believe that this overestimation is largely due to: (1) the poor quality of available subsurface data at these two sites, and (2) local boundary effects. The penetration tests at Mission Creek and South of Market were performed with a non-standard hammer and no grain-size distribution data are available (O'Rourke et al., 1991). We converted the non-standard penetration resistances to SPT N values and used estimated soil properties for our liquefaction analyses, but these estimates are suspect. Also, ground displacement at these sites were inhibited by lateral boundary effects. The ground failure at Mission Creek formed in a narrow, sinuous, old, creek channel which caused the lateral spread to change directions at several junctures along its path (O'Rourke et al., 1991). These directional changes undoubtedly impeded the ground displacement.

5.11 Flow Chart for the Application of Equation 4.1.9

Figure 5-9 summarizes the suggested procedure for applying the MLR model. In summary, Equation 4.1.9 yields the best results for $6.0 \leq \mathbf{M} \leq 8.0$ earthquakes and at sites underlain by continuous layers of sands and silty sands having $\mathbf{N1_{60S}} \leq 15$; $0.075 \leq \mathbf{D50_{15}} \leq 1.0$ mm, $0 \leq \mathbf{F_{15}} \leq 50$ %, $1 \leq \mathbf{T_{15}} \leq 15$ m, $1 \leq \mathbf{W} \leq 20$ %, and $0.1 \leq \mathbf{S} \leq 6$ %. Also, the depth to the bottom of the liquefied layer, $\mathbf{Z_{BLS}}$, should be found within the upper 20 m of the profile. In addition, because this model was developed from western U.S. and Japanese sites founded primarily on stiff soils,

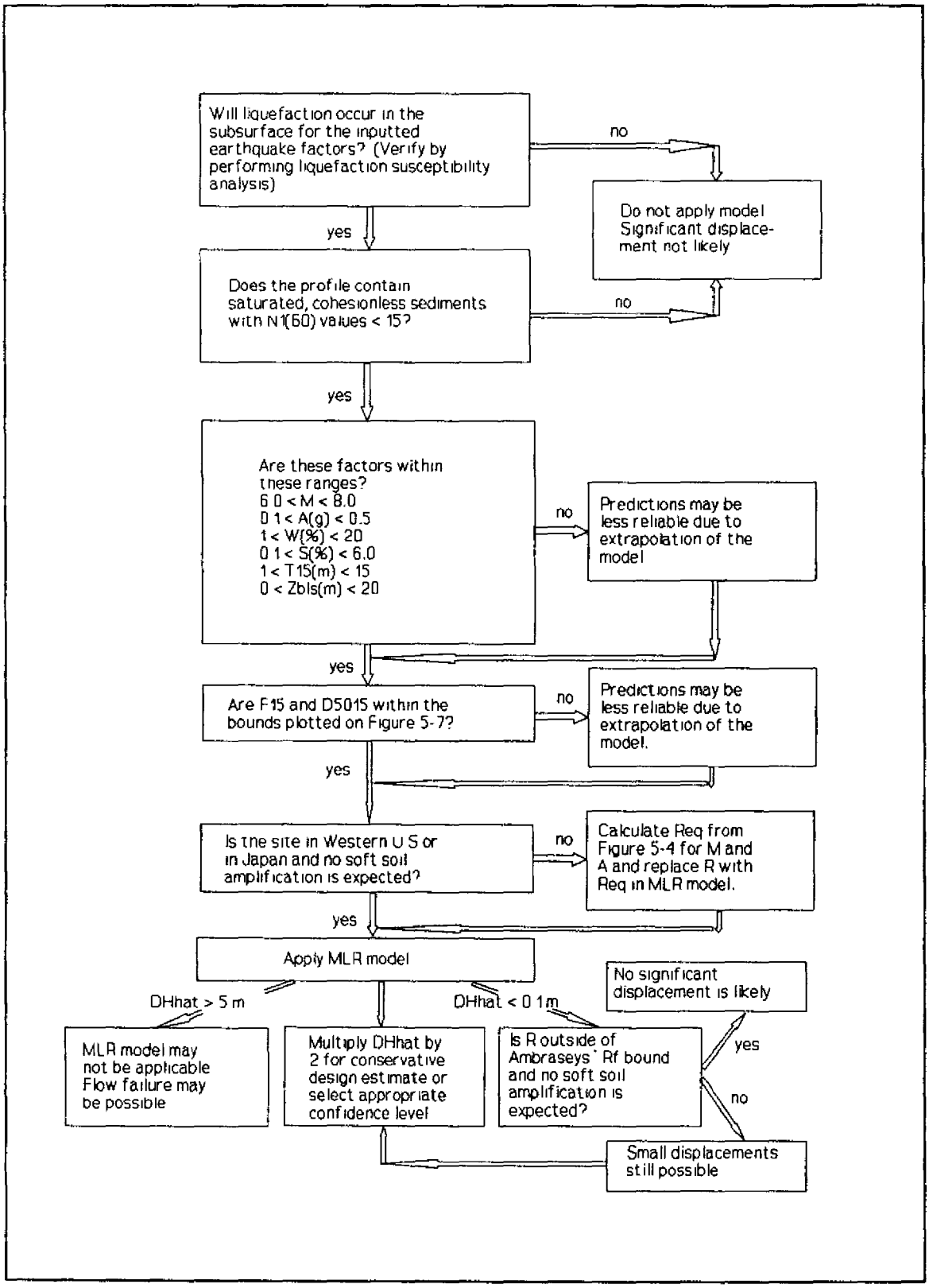

Figure 5-9 Flow chart for the application of Equation 4.1.9

it is most applicable to these soil conditions and to seismic regions having high to moderate ground motion attenuation. However, Figure 5-4 may be used to adjust the value of R used in the model so that it can be applied to other regions with different seismic attenuation or to sites where significant soft soil amplification is expected.

5.12 Calculation of the Upper Prediction Limit for Displacement

Although D_{Hhat} is an estimate of the mean displacement for a given set of $\mathbf{X(s)}$, it is often desirable to determine an upper bound or limit to the amount of displacement that can be reasonably expected at a given site. Figure 4-4 shows that almost all values of D_{Hhat} calculated from Equation 4.1.9 fall below the "MEASURED = 2 X PREDICTED LINE." This suggests that if D_{Hhat} is multiplied by a factor of 2, then that result will provide a conservative estimate of D_H that is not likely to be exceeded. However, MLR models offer a more rigorous, probabilistic approach to calculating the upper prediction limit or bound for the true response. For example, a 90 percent prediction limit forms the bound where it is expected that 90 percent of the observed displacements will be less than the bound and 10 percent will exceed the bound. The predicted value,

$$D_{Hhat} = b_0 + b_1X_1 + \ldots + b_pX_p, \tag{5.12.1}$$

is a best-fit estimate of

$$E(D_H) = B_0 + B_1X_1 + \ldots + B_pX_p \tag{5.12.2}$$

where:
$E(D_H)$ is the mean or expected value of D_H.

The variance of D_{Hhat}, i.e., $V(D_{Hhat})$, is calculated from:

$$V(b_0) + X_{12}\,V(b_1) + \ldots + X_p^2\,V(b_p) + 2X_1\,\text{covar}\,(b_0,b_1) + \ldots + 2X_{p-1}X_p\,\text{covar}\,(b_{p-1},b_p) \tag{5.12.3}$$

where: "covar" is the covariance.

This expression is solved in matrix notation as follows (Draper and Smith, 1981):

$$V(D_{Hhat}) = \sigma^2(X_0'CX_0) \tag{5.12.4}$$

where:
σ = standard deviation of D_H and is estimated by the standard deviation of the regression model, $\mathbf{s}$. The $\mathbf{s}$ for Equation 4.1.9 is 0.207 (i.e., $\mathbf{s}$ = (MS error)$^{1/2}$ from the Analysis of Variance Table for Equation 4.1.9, see Appendix 2).

The matrix, X_0, contains the site-specific values of the $\mathbf{X(s)}$ used to calculate D_{Hhat}:

$$X_0' = [1, X_1, \ldots, X_p] \tag{5.12.5}$$

and the C matrix is the variance-covariance matrix:

$$\begin{matrix} C_{00} & C_{01} & \ldots & C_{0p} \\ C_{10} & C_{11} & \ldots & C_{1p} \\ \ldots & \ldots & \ldots & \ldots \\ C_{p0} & C_{p1} & \ldots & C_{pp}. \end{matrix} \tag{5.12.6}$$

The C matrix is calculated from the matrix operation:

$$(X'X)^{-1} \tag{5.12.7}$$

where:
X is the matrix comprised of the set of **X(s)** used in fitting the regression model.

The C matrix for Equation 4.1.9 has been tabulated in the file C.DAT on the computer disk labelled Appendix 3 which is available from NCEER.

The 1-α upper prediction limit for the true displacement is given by (Draper and Smith, 1981):

$$D_{Hhat} + t_{((n-p-1),\,1-\alpha)} * s * (1 + X_0'*C*X_0)^{1/2}. \qquad (5.12.8)$$

where:
α is selected by the evaluator and is called the significance level.

For example to calculate the 90 percent upper prediction limit for the true displacement, then 1-α equals 0.90 and α equals 0.10. The critical t-value for the selected 1-α value is determined from the t distribution for n-p-1 degrees of freedom (Table 5-2). Equation 4.1.9 has 457 degrees of freedom, (n = 467, p = 10). Because t-values are not usually tabulated for 457 degrees of freedom, the critical t-values corresponding to 400 degrees of freedom have been listed in Table 5-2. (The use of t_{400} critical values has very little impact on the final answer because t_{457} is closely approximated by t_{400}.)

As an example of the application of Equation 4.1.9 and Equation 5.12.8, we will calculate the 90 percent upper prediction limit for true value of D_H at borehole 5-42, in Niigata (see Figure 3-2). Because this is a ground slope failure, we will apply Equation 4.1.9b and the following values of the **X(s)** to form the X_0 matrix: (1, 0, **M** = 7.5, **LOG R** = 1.32, **R** = 21, **LOG** W_{ff} = 0, **LOG** S_{gs} = -0.699, **LOG** T_{15} = 0.477, **LOG**$(100-F_{15})$ = 1.978, $D50_{15}$ = 0.433). The predicted value for **LOG**(D_H + 0.01) from Equation 4.1.9 is -0.03275 and:

$$D_{Hhat} = 10^{-0.03275} - 0.01 = 0.917 \text{ m}. \qquad (5.12.9)$$

To calculate the 90 percent upper predict limit for D_H, we first form the X_0' matrix:

$$X_0' = [1,\ 0,\ 7.5,\ 1.32,\ 21,\ 0,\ -0.699,\ 0.477,\ 1.978,\ 0.433] \qquad (5.12.10)$$

The first two elements in this matrix, {1,0}, are called dummy variables (Draper and Smith, 1981). The first element, {1}, indicates that b_0 applies to the ground slope component of the model, and the second element, {0}, indicates that b_{0ff} does not apply. Next, we perform the matrix operation $X_0'CX_0$:

$$X_0'CX_0 = 0.0213. \qquad (5.12.11)$$

The 90 percent upper prediction limit is calculated from equation 5.12.8:

$$LOG(D_{H90}) = -0.03275 + 1.284 * 0.207 * (1+0.0213)^{1/2} = 0.236 \qquad (5.12.12)$$

or

$$D_{H90} = 10^{0.236} - 0.01 = 1.712 \text{ m}. \qquad (5.12.13)$$

Thus, we conclude that we are 90 percent confident (i.e., 90 percent probability) that the true value of D_H at borehole 5-42 will not exceed 1.712 m.

Similarly, we can calculate the 90 percent upper prediction limit for true value of D_H at borehole G10-39 (Figure 3-2). Because this is a free face failure, we apply Equation 4.1.9a and the following values of **X(s)** to form the X_0 matrix: (1, 1, **M** = 7.5, **LOG R** = 1.32, **R** = 21, **LOG** W_{ff} = 0.477, **LOG** S_{gs} = 0, **LOG** T_{15} = 1.114,

$LOG\ (100-F_{15})$ = 1.982, $D50_{15}$ = 0.400. The predicted value of $LOG(D_H + 0.01)$ from Equation 4.1.9a is 0.27241 and:

$$D_{Hhat} = 10^{0.27241} - 0.01 = 1.862 \text{ m.} \qquad (5.12.14)$$

The X_0' matrix is:

$$X_0' = [1,\ 1,\ 7.5,\ 1.32,\ 21,\ 0.477,\ 0,\ 1.114,\ 1.982,\ 0.400] \qquad (5.12.15)$$

The dummy variables for the first two elements in this matrix, {1,1}, indicates that both b_0 and $b0_{ff}$ apply to the free face component of the model. The value of $X_0'CX_0$ equals 0.0151, and the 90 percent upper prediction limit is:

$$LOG(D_{H90}) = 0.27241 + 1.284 * 0.207 * (1+0.0151)^{1/2} = 0.540 \qquad (5.12.16)$$

or

$$D_{H90} = 10^{0.540} - 0.01 = 3.459 \text{ m.} \qquad (5.12.17)$$

Thus, we are 90 percent confident that the true value of D_H at borehole 5-42 will not exceed 3.459 m.

Other upper prediction limits, besides the 90% upper prediction limit used in the above example, can be calculated by simply selecting the desired confidence level from Table 5-2 and using that value in Equation 5.12.8 for $t_{((n-p-1),\ 1-\alpha)}$.

TABLE 5-2
CRITICAL t VALUES FOR CONFIDENCE LIMITS
(based on 400 degrees of freedom, after Ostle and Malone, 1988)

Confidence level (1-α) in percent						
75%	80%	85%	90%	95%	97.5%	99.5%
0.676	0.843	1.038	1.284	1.649	1.966	2.588

5.13 Comparison of Equation 4.1.9 with Other Empirical Models

We applied the LSI model proposed by Youd and Perkins (1987) and the slope-thickness model of Hamada et al. (1986) to our compiled data and compared the performance of these models with Equation 4.1.9 (Figure 5-10). The LSI model (Equation 2.7.1.3) conservatively bounds almost all of the U.S. data, but underestimates many of the displacement vectors measured in Niigata and Noshiro, Japan. There are a few plausible reasons for this underprediction of the Japanese data by the LSI. First, the LSI was primarily developed from U.S. case studies where subsurface conditions were generally less favorable to widespread liquefaction. Thus, the LSI does not adequately reflect the high liquefaction susceptibility of the soils found in Niigata and Noshiro, Japan. Second, the location of the seismic source for the 1964 Niigata and 1983 Nihonkai-Chubu earthquakes is not well known. Both of these subduction zone earthquakes occurred in the Japan Sea where the faulting is not well understood. We estimate that R was approximately 21 and 27 km, respectively from Niigata and Noshiro cities, based on studies of crustal warping in the Japan Sea (Mogi et al., 1964; Hwang and Hammack, 1984). However, if R was indeed closer than our estimates, then the LSI would bound much more of the Japanese data.

The thickness-slope model proposed by Hamada et al. (Equation 2.7.2.8) performs adequately for Niigata and Noshiro, Japan, but tends to overpredict many of the displacements measured at U.S. sites (Figure 5-10). The R^2 for this model is 35.1 percent and 73 percent (329 of 448) of the predicted observations fall between the upper and lower prediction bounds. (To be consistent with the techniques used by Hamada et al. in developing this model, we modified our liquefaction analysis program to calculate the thickness of the liquefied layer, H, using the liquefaction susceptibility curves outlined by the Japanese Code of Bridge Design (Section 2.7.2). We also measured θ in a manner that was consistent with the definition proposed by Hamada et al. (Figures 2-2a and 2-2b.)) There are a few possible reasons why the Japanese model tends to perform poorly at many U.S. sites. First, the earthquakes that generated lateral spread in the U.S. were significantly different from those that struck Niigata and Noshiro. Niigata and Noshiro experienced very similar earthquakes (M = 7.5 and 7.7, respectively) and the seismic sources were located approximately the same distance from the two cities (approximately 21 and 27 km, respectively). In contrast, the U.S. case studies include earthquakes that range from $6.6 \leq M \leq 9.2$, and lateral spread sites that were located at varying distances from the seismic source ($0.2 \leq R \leq 100$ km). Second, the liquefied sediments in Niigata and Noshiro tend to be relatively clean compared to many U.S. sediments that are more silty. Third, our techniques of measuring H and θ may not be entirely consistent with those used by the Japanese investigators in reducing their data.

Based on the performance of Equation 4.1.9 as shown in Figure 5-10, we conclude that our attempt to formulate a more comprehensive MLR model for predicting lateral spread displacement has been successful. Because our model is derived from and adjusted for a wider range of seismic, site, and soil conditions than the previously proposed empirical models, it is more general and will yield better results if properly applied.

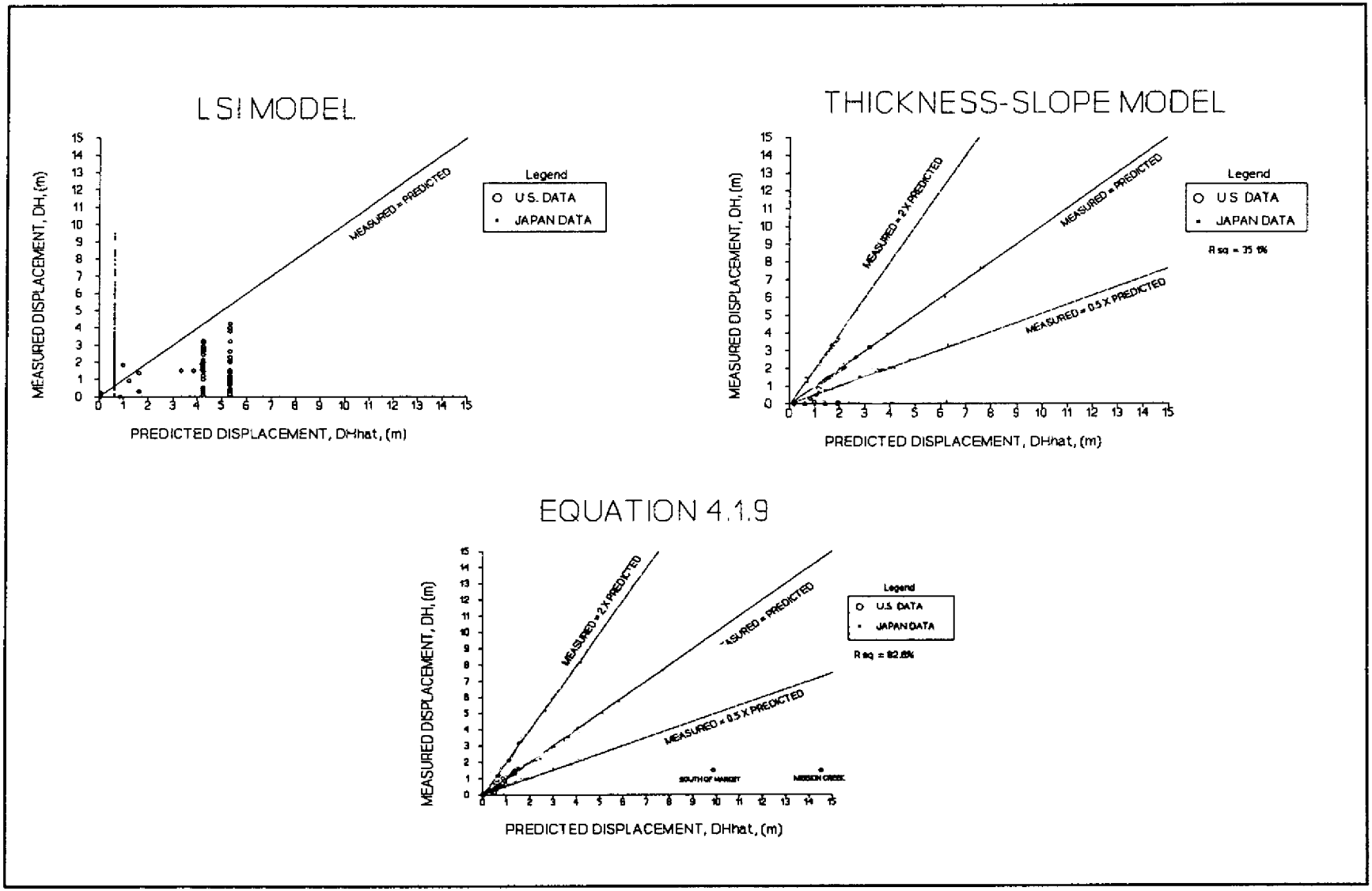

Figure 5-10 Comparison of D_H versus D_{Hhat} for LSI model, Hamada et al. thickness-slope model, and Equation 4.1.9 showing improved performance of Equation 4.1.9.